Polym. Bull.
https://doi.org/10.1007/s00289-018-2277-2

ORIGINAL PAPER

High performance polyvinyl alcohol/calcium titanate nanocomposite anion-exchange membranes as separators in redox flow batteries

P. P. Moly[1] · C. B. Jeena[1] · P. J. Elsa[1] · K. J. Ambily[1] · V. T. Joy[1]

Received: 20 June 2017 / Revised: 22 November 2017 / Accepted: 10 January 2018

Abstract Low ionic conductivity and poor chemical stability are the two key parameters that limit the use of many anion-exchange membranes in electrochemical applications like rechargeable batteries and fuel cells. Herein we report a method for the synthesis of a high performance anion-exchange membrane fabricated by incorporating calcium titanate nanoparticles ($CaTiO_3$) into polyvinyl alcohol (PVA) matrix. The $CaTiO_3$ was synthesized by a new co-precipitation method from a solution of two simple precursors, viz potassium titanyl oxalate and calcium chloride. The XRD data of the synthesized nanoparticles indicate a phase pure orthorhombic perovskite structure. Morphological features investigated with SEM and TEM studies, reveal that the $CaTiO_3$ is having spherical shape with a diameter of approximately 200 nm. The PVA/$CaTiO_3$ nanocomposite membranes were fabricated by solution casting method from a well dispersed suspension of $CaTiO_3$ in PVA and characterized by FT-IR spectroscopy, TGA, SEM, AC impedance analysis and tensile strength measurements. The membranes with 30 wt% $CaTiO_3$ content possess ionic conductivity of 66 mS cm^{-1} at room temperature. The electrochemical performance of an all-iron redox flow cell was studied using galvanostatic charge–discharge tests using the above nanocomposite membrane as separator and the system exhibited a coulombic efficiency of 75% during the charge–discharge cycles.

Keywords Calcium titanate · Anion-exchange material · PVA/$CaTiO_3$ nanocomposite · Anion-exchange membranes · All-iron redox flow battery

✉ V. T. Joy
joyvthomas2002@gmail.com

[1] P. G. and Research Department of Chemistry, Christ College (Autonomous), Irinjalakuda, Affiliated to University of Calicut, Irinjalakuda, Kerala 680125, India

Published online: 17 January 2018

Introduction

The ion-exchange membrane is a critical component of many electrochemical devices such as fuel cells [1], rechargeable batteries [2], electrodialysis devices [3], water electrolysers and desalination of sea water [4] as it determines the performance as well as the economic viability of these devices. The membrane allows selective transport of either cation or anion to complete the circuit during the passage of current [5–10]. Recently, in fuel cell technology anion-exchange membranes (AEMs) are gaining more attention as they promise to overcome the disadvantages such as low CO tolerance, high electrokinetic over potentials for oxygen reduction and high catalyst cost of proton exchange membrane fuel cells (PEMFCs) [11–13]. The cost of popular proton exchange membrane Nafion is roughly \$400 per m^2 [13]. However, the currently used commercial AEMs suffers from severe drawbacks, which includes low ionic conductivity, electrolyte crossover, poor chemical and mechanical stability besides high cost of the membranes [14–18]. Various kinds of AEMs have been developed in the past few decades and most of them employed quaternary ammonium group as anion exchange cites [19, 20]. These quaternary ammonium group-based membranes degrade rapidly in highly alkaline solutions and hence limits the performance of these membranes in alkaline environment [13, 17]. So the developments of low-cost AEMs with superior chemical stability and good ionic conductivity have been the focus of research of many groups worldwide.

Organic–inorganic hybrid membranes were found to be promising materials for potential applications due to their better electrochemical properties, improved mechanical, chemical and thermal properties [21]. Yang synthesized PVA/TiO_2 composite polymer membrane [18] and quaternized poly(vinyl alcohol)/alumina composite polymer membranes [22] for alkaline direct methanol fuel cells, which exhibited excellent electrochemical performances. The incorporation of ceramic fillers such as Al_2O_3 [22], SiO_2 [23] and bentonite [24] into the polymer matrix has significantly enhanced the ionic conductivity and thermal stability of the ion-exchange membranes.

The AEMs based on PVA have received considerable attention in recent years due to its non toxicity, good film-forming ability, low cost, good mechanical strength and chemical stability, high hydrophilic behavior and low methanol permeability [18, 25, 26]. The incorporation of nanofiller into the polymer matrix of cross-linked PVA have been shown to reduce the crystalline nature of the matrix and improve their performance in solid alkaline fuel cells and other electrochemical devices [18, 25–27].

A perovskite is any material with the same type of crystal structure as calcium titanate ($CaTiO_3$). The general chemical formula of perovskite is ABX_3, where A represents large divalent and B is small tetravalent cation. X can be anions like O^{2-} which is bonded to both cations. Synthesis of calcium titanate nanocrystals have gained great interest in recent years due to their exceptionally high dielectric properties which makes them potentially useful resonator materials in wireless communication systems [28, 29]. Calcium titanate can exist in three polymorphic

phases including cubic, tetragonal and orthorhombic [30]. Zr^{4+} doped $CaTiO_3$ and CoO doped $CaTiO_3$ powders exhibit high catalytic efficiency in water splitting for hydrogen production [31]. Due to inherent biocompatibility, calcium titanate is highly beneficial for biomedical applications, especially for bone and joint repair [32].

Several methods have been reported for the synthesis of calcium titanate nanoparticles such as solid state synthesis, sol–gel methods, hydrothermal methods, co-precipitation methods, mechanical alloying methods, solvo-thermal methods [31–33]. The limitations associated with these processes are heterogeneous products, contamination of impurities, performing the process at high temperature (above 1300 °C) and existence of coarse particles with different size [33]. Calcium titanate, when treated with bases in wet condition is converted to calcium titanate hydroxide (Eq. 1) and it is reported to be an efficient anion-exchange material containing exchangeable hydroxyl groups [34]:

$$CaTiO_3 + NaOH \rightarrow HCaTiO_3OH. \quad (1)$$

In this work, calcium titanate nanoparticles were synthesized by a new method from a solution containing two simple precursors, viz potassium titanyl oxalate and calcium chloride using ammonium oxalate as precipitating agent. The powder was calcined at 900 °C and characterized by XRD, TEM, SEM, and EDX analysis.

The AEMs were fabricated by incorporating calcium titanate nanocrystals to PVA matrix followed by cross-linking with glutaraldehyde. The membranes were characterized by FT-IR, TGA, SEM, and AC impedance analysis. The membrane properties such as the alkaline stability, water uptake, ion-exchange capacity and mechanical strength were also measured.

Experimental

Materials

PVA used in this study was analytical grade and was purchased from Merck (M_w 89,000–98,000, 99+% hydrolysed PVA). Glutaraldehyde (25 wt% solution in water of analytical grade), calcium chloride, potassium titanyl oxalate, and ammonia solution were also purchased from Merck.

Preparation of calcium titanate nanopowder

Potassium titanyl oxalate (0.02 mol) and calcium chloride (0.02 mol) were separately dissolved in 250 ml D. I. water. The solutions were mixed and 250 ml of 0.03 M ammonium oxalate was slowly added to the mixture under stirring at room temperature and then pH of solution was adjusted to 9 by adding 25% ammonia solution. The white oxalate hydroxide slurry formed was aged overnight. It was then filtered, washed with D. I. water until pH was neutral and dried at 80 °C

in an air oven for 48 h. The product was calcined at 900 °C for 2 h. The synthesis procedure is shown as follows:

$$K_2[TiO(C_2O_4)_2] \cdot 2H_2O \xrightarrow{(NH_4)_2C_2O_4,\ NH_4OH} CaTi(OH)_x(C_2O_4)_y \xrightarrow[C]{900^\circ} 2\,hCaTiO_3 \quad (2)$$

Fabrication of PVA/calcium titanate nanocomposite membranes

5 wt% PVA solution was prepared by dissolving 5 g PVA in 100 ml D. I. water at 80 °C and it was stirred continuously till a homogeneous solution was obtained. Then a weighed amount of calcium titanate was ultrasonicated for 6 h and stirred with PVA solution for another 6 h. Then glutaraldehyde solution (5 wt%) as the crosslinker was added drop wise (2.5 wt% of PVA) into the mixture [8] followed by several drops of 1 M HCl as catalyst. After stirring for 3 h the mixture was degassed in vacuum for 15 min. The viscous solution was cast onto a clean glass plate using a film applicator. The composite membranes were peeled from the glass plate after drying in vacuum oven at 50 °C for 48 h. PVA/*x*$CaTiO_3$ composite membranes (*x* stands for the wt% of $CaTiO_3$) were prepared at PVA/$CaTiO_3$ weight ratios (95:5, 90:10, 85:15, 80:20, and 70:30) and the corresponding membranes are denoted as PVA5, PVA10, PVA15, PVA20 and PVA30. The thickness of the resulting membranes was 120 ± 10 μm. All the membranes were immersed in 2 M NaOH solution for 24 h for converting calcium titanate to calcium titanate hydroxide which is an efficient anion exchange material containing exchangeable hydroxyl groups [34].

Characterization

X-ray powder diffraction data of the synthesized nanopowder were collected at room temperature with a SHIMADZU, XRD700 powder diffractometer using CoK_α radiation. Data were scanned over the angular range 20°–80° (2θ) with a step size of 0.0196° (2θ). Transmission electron microscopy (TEM) images of the obtained nanoparticles have been recorded using a JEOL 4000EX High Resolution Transmission Electron Microscope (HRTEM) operated at 400 kV. FT-IR spectra were recorded on a Perkin Elmer instrument (Model L160000A) over a range of 4000–400 cm^{-1}. SEM images of the samples were acquired with a scanning electron microscope (JSM-5600, JEOL Co., Japan). The samples were coated with a thin layer of gold by ion sputtering prior to microscopic examination. The energy dispersive analyzer was used for the elemental detection of the samples. TGA thermograms of the composite membranes were recorded on a Shimadzu TGA-50H analyzer by heating the samples from room temperature to 850 °C under nitrogen atmosphere at a heating rate of 10 °C/min.

Water uptake of the composite membranes was determined by weighing the membranes under wet conditions after being equilibrated in distilled water for 24 h at room temperature. The surfaces of the membranes were then carefully wiped with filter paper and the membranes were weighed immediately. The samples were

vacuum dried for 2 days and weighed again. The water uptake was calculated as follows:

$$\text{Water uptake } (\%) = \frac{W_{\text{wet}} - W_{\text{dry}}}{W_{\text{dry}}} \times 100\%, \tag{3}$$

where W_{wet} is the mass of the water swollen membrane, and W_{dry} is the mass of the dry membrane.

The ion exchange capacities (IECs) of the composite membranes were determined by double titration method. Samples were accurately weighed and immersed in 25 ml of 0.05 M HCl solution for 48 h and the HCl solution was back titrated by 0.05 M NaOH solution using phenolphthalein as indicator.

IECs of the samples were calculated using the equation:

$$\text{IEC} = \frac{n_1 \cdot \text{HCl} - n_2 \cdot \text{HCl}}{M_{\text{dry}}}, \tag{4}$$

where n_1 of HCl and n_2 of HCl are the concentrations of (mmol) hydrochloric acid required before and after equilibrium, respectively, and M_{dry} is the mass in g of the dried sample. The average value of the three samples calculated from the above equation is the IEC value of the membrane.

Electrochemical impedance spectroscopy (EIS) was used to evaluate ionic conductivity of the membranes, using AUTOLAB 50519 PGSTAT instrument. Impedance of the membranes were performed in a two electrode setup where the membranes were clamped between two platinum electrodes and the cell was thermostated at 25 ± 0.1 °C for at least 20 min to ensure thermal equilibrium. Impedance measurements were performed in the frequency range 100 Hz–1000 kHz using an alternating potential of amplitude 10 mV. Fully hydrated membrane was placed in the conductivity cell and it was filled with 2 M NaOH. The resistance of the membrane and solution (R_{total}) was measured. The resistance of the solution (R_{solution}) was measured without the membrane. Membrane resistance (R_{mem}) was obtained from the difference of the measured resistances ($R_{\text{mem}} = R_{\text{total}} - R_{\text{solution}}$). The thickness of the membrane was measured with a digital micrometer by placing the membrane between two glass slides to ensure both a planar surface and limited compression. The conductivity of the membrane was calculated as follows $\sigma = L/RA$ mS cm^{-1}, where σ is the hydroxide conductivity in mS cm^{-1}, R is the ohmic resistance of the membrane (Ω), L is the thickness of the membrane (in cm), A is the cross sectional area of membrane samples (cm^2).

The tensile strength of the composite membranes was measured with universal testing machine (UTM) (Zwick, Model 1446-60, Germany). For this test the samples were prepared according to ASTM-D882 standard. The films were then placed between the grips of the testing machine. The grip length was 5 cm and speed of testing was set at the rate of 10 mm min^{-1}. The alkaline stability of the membrane was measured by immersing the composite membrane sample with a size of 3 cm × 3 cm in 2 M aq. NaOH at room temperature for 2 weeks. It was taken out, washed with D. I. water, wiped with tissue paper, and then studied using FT-IR technique to detect any degradation or changes in chemical structures. Loss of

weight of the membrane was also measured. The oxidative stability of membrane was determined by immersing the samples 3 cm × 3 cm into Fenton's reagent (30 ppm $FeSO_4$ in 30% H_2O_2) at 25 °C, for 24 h and measured the weight of the membrane with time.

Performance of $CaTiO_3$/PVA membrane as separator in all-iron flow battery

All-iron flow battery experiments were performed in the 36 cm^2 flow cell hardware with electrolyte flowing across two electrodes, separated by the membrane prepared [35]. All experiments were performed with electrolyte flow rates of 25 ml min^{-1}. Electrolyte for both positive and negative electrodes consisted of 1 M $FeCl_2$ and 1.5 M NH_4Cl. The electrodes were made from densified graphite with a cross-sectional area of 16 cm^2. The charging efficiency of the all-iron redox flow cell was determined by charging the cell at 100 mA cm^{-2} for 100 s followed by discharging at 50 mA cm^{-2} using AUTOLAB 50519 PGSTAT instrument. The cell performance is normally determined by its coulombic efficiency (CE). CE is the ratio of discharge capacity (Q_{dis}) to charge capacity (Q_{ch}) of a cell.

Results and discussion

Figure 1 shows the XRD pattern of $CaTiO_3$ obtained after calcination at 900 °C. Diffraction patterns of calcium titanate powder obtained well correlates with standard (JCPDS No. 22-153) and dominant peaks are obtained at $2\theta = 32.7$, 47.1, 58.9, and 69, which corresponds to diffraction from (121), (202), (123), (242) planes. The XRD pattern clearly shows that the powder obtained by the thermal decomposition of ($CaTi(OH)_x(C_2O_4)_y$) at 900 °C consists of pure perovskite nanopowder ($CaTiO_3$) without the presence of oxides or any other impurity [30].

The microstructure of the particles was also investigated by means of TEM. Figure 2 shows the TEM image of $CaTiO_3$ and reveals the particle morphology and

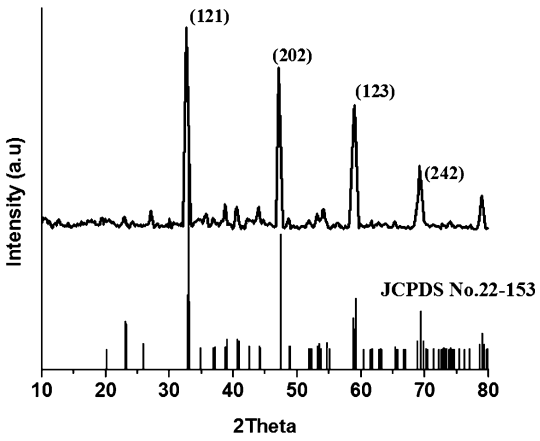

Fig. 1 XRD pattern of calcium titanate

size of the nanopowder. It is seen from TEM images that $CaTiO_3$ powders consist of clusters of nanoparticles and they are found to be spherical in shape with an average size of 200 nm. HRTEM image of calcium titanate Fig. 2c reveals the formation of nano-crystals with d spacing of 0.32 nm. The selected area electron diffraction (SAED) pattern given in Fig. 2d reveals the crystalline nature and the rings in the SAED pattern corresponds to crystal planes of calcium titanate.

Structural analysis

FT-IR spectra of $CaTiO_3$, PVA, PVA10, PVA20 and PVA30 nanocomposite membranes are presented in Fig. 3a–e. Figure 3a shows two characteristic peaks at 540, 450 cm^{-1} in the spectrum of $CaTiO_3$ which correspond to the stretching vibrations of Ti–O bonds [36] and Ca–Ti–O bending vibrations [37], respectively. Figure 3b shows the characteristic peaks of pure PVA in the region

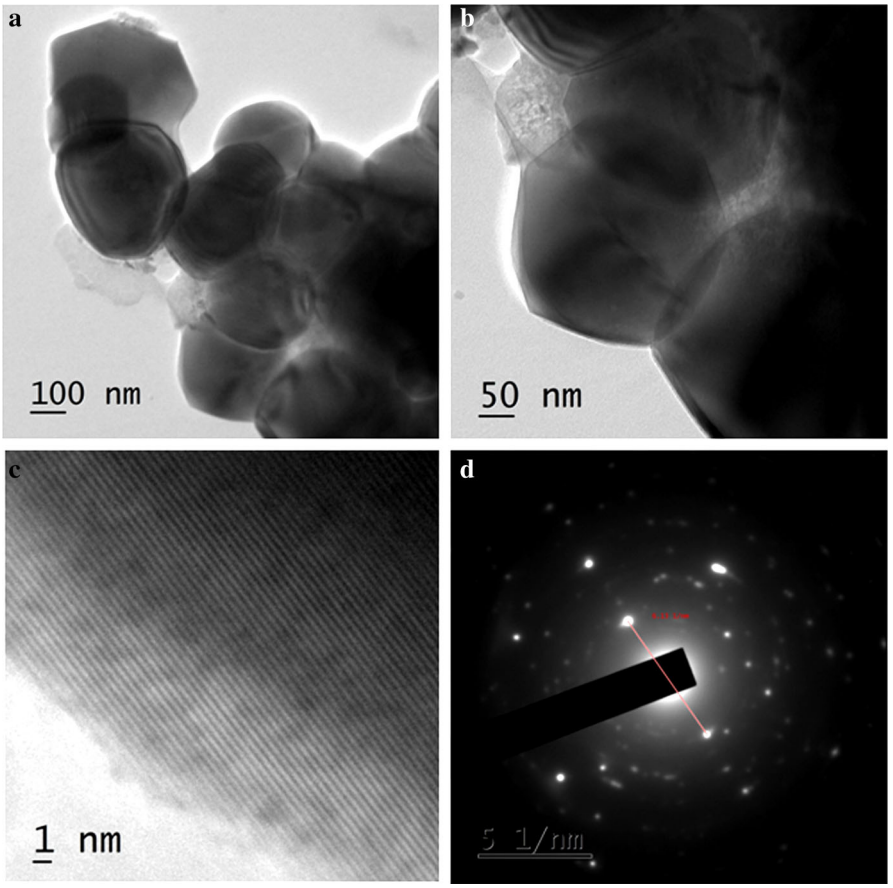

Fig. 2 **a**, **b** TEM images of calcium titanate at different magnifications, **c** HRTEM image of calcium titanate nanocrystals, **d** SAED pattern of calcium titanate

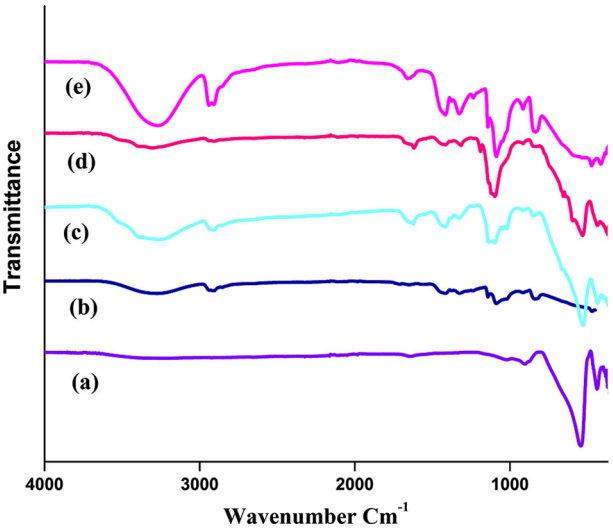

Fig. 3 FT-IR spectra of (a) $CaTiO_3$, (b) PVA, (c) PVA10, (d) PVA20 and (e) PVA30 nanocomposite membranes

3400–3100 cm^{-1} due to –OH stretching, band at 2920 cm^{-1} due to –CH stretching vibrations of polymer back bone and band at 1420 cm^{-1} is attributed to bending vibrations of $–CH_2$ group as reported in literature [38, 39]. Figure 3c–e of PVA10, PVA20 and PVA30 nanocomposite membranes show broad peak at 3400–3100 cm^{-1} indicates stretching vibrations of the hydroxyl groups of polyvinyl alcohol. The band at 2924 cm^{-1} is assigned to the stretching vibrations of –CH groups of polymer back bone and bands at 1420 cm^{-1} is attributed to bending vibrations of $–CH_2$ group [40]. The bands at 1250–1200 cm^{-1} were attributed to the ether bonds (C–O–C), formed during cross-linking with glutaraldehyde [39]. In the composite membrane, the peaks at 540 and 450 cm^{-1} is attributed to the characteristic vibrations of Ti–O bonds and Ca–Ti–O bonds of calcium titanate [37]. The results show that successful incorporation of calcium titanate nanoparticles into the PVA matrix has been achieved.

SEM analysis

The SEM images of calcium titanate are shown in Fig. 4. The SEM image shows the microstructure of the particles. The images revealed the information about grain size, shape and powder agglomeration. The particles are found to be spherical in shape and are highly agglomerated. The average size of the particles was in 200 nm range. The EDX spectrum of calcium titanate in Fig. 5 indicates the presence of Ca, Ti and O atoms in accurate proportion in the prepared material, further confirmed the formation of pure calcium titanate.

Figure 6a–d present the SEM images of surface and cross-section of PVA/$CaTiO_3$ nanocomposite membranes. There is no evidence of phase separation; crack or holes on membrane surface indicated its dense nature, which was further

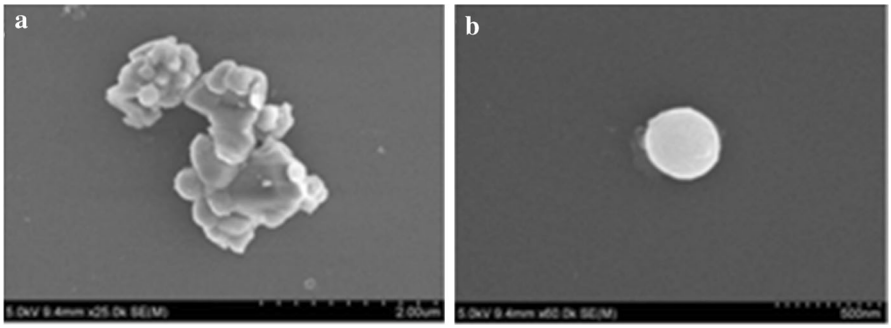

Fig. 4 **a**, **b** SEM images of calcium titanate with different magnifications

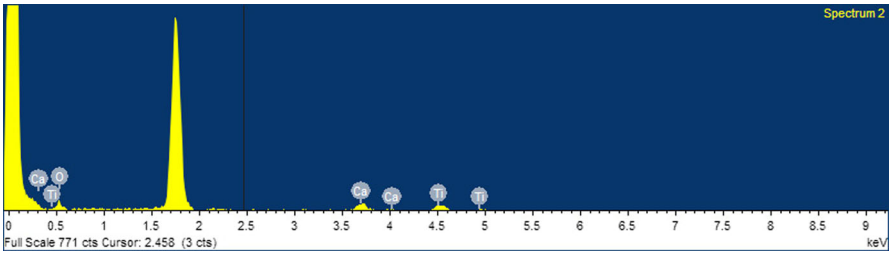

Fig. 5 The EDX spectrum of calcium titanate

confirmed by cross-section image of the membrane. The surface of the membrane found to be smooth and uniform. Filler particles are found to be well embedded in the polymer matrix, establishing strong connectivity of the particles. Size of the filler particles embedded in the PVA matrix is found to be less than 1 μm and some degree of aggregation of particles are observed. The particle distribution and particle–polymer matrix reinforcement play vital roles in the improvement of the mechanical properties of the composite membranes. The distribution of particles is uniform and homogenous when the weight percent of nano $CaTiO_3$ filler is less than 20 wt%. When the filler content is beyond a limit, aggregates of filler particles make the membrane more brittle [5]. Cross-sectional SEM image of PVA30 membrane shows that the thickness of the membrane is about 120 ± 10 μm.

Water uptake

It is found that water uptake decrease with increase in calcium titanate content. This can be explained in terms of the changes in the membrane structure. Cross-linking effects due to the inorganic network reduce polymer chain mobility thereby reducing the free volume where absorbed water could be accommodated. Here, the cross-linking effect due to the inorganic network is more prominent than the hygroscopic effect of $CaTiO_3$, and hence the total water content decreases with

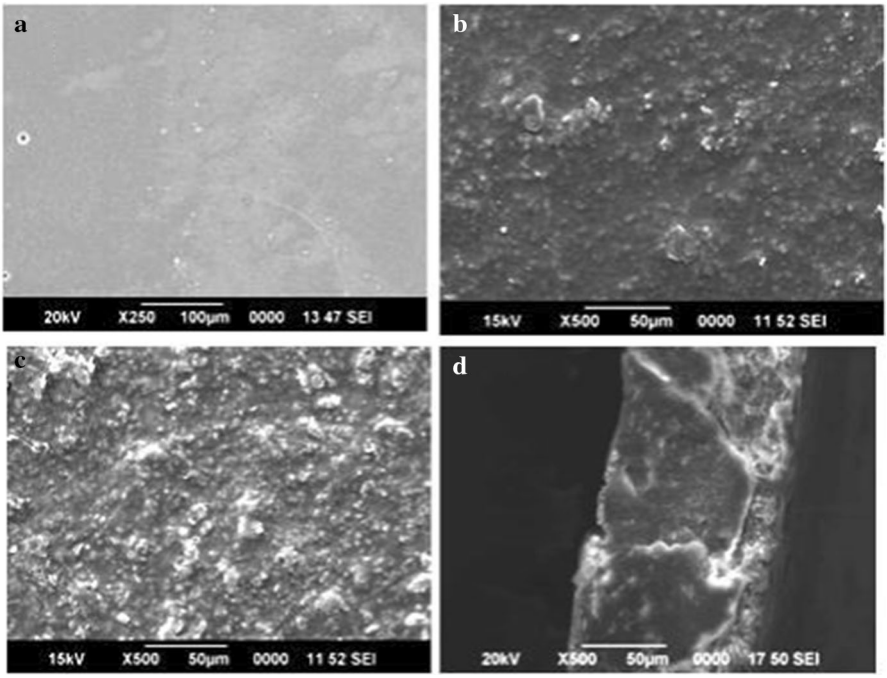

Fig. 6 SEM surface images of membranes; **a** PVA, **b** PVA10, **c** PVA30, **d** SEM cross-sectional image of PVA30 membrane

increasing $CaTiO_3$ content [18, 40, 41]. The decrease in water uptake with increase in calcium titanate content also indicates the dimensional stability of composite membranes (Fig. 7; Table 1).

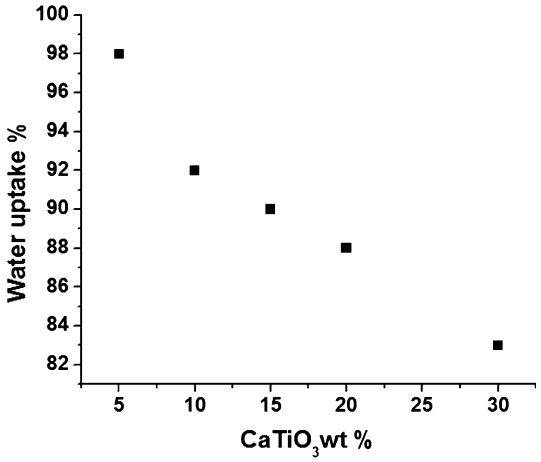

Fig. 7 Water uptake of membranes with varying $CaTiO_3$ content

Table 1 The physical properties of PVA/$CaTiO_3$ nanocomposite polymer membranes at 25 °C

Types of membranes	Water uptake (%)	IEC (meq g^{-1})	Tensile strength (M Pa)	Ionic conductivity (mS cm^{-1})
PVA0	116	0.38	13.6	8.2
PVA5	98	0.42	20	14
PVA10	92	0.56	25	25
PVA15	90	0.58	40	32
PVA20	88	0.64	46	39
PVA30	83	0.78	25	66

Ion exchange capacity (IEC)

The IEC is a key parameter for the characterization of ion exchange membrane and it has an intensive effect on the water uptake as well as ionic conductivity of the membranes [21, 42]. IEC provides an indication of amount of exchangeable groups in the membrane [3]. Figure 8 shows ion exchange capacity of membranes with varying $CaTiO_3$ content. It is found that ion exchange capacities increased gradually with increasing $CaTiO_3$ content in the composite membrane. The ion exchange capacity values of the membranes were in the range of 0.4–0.7 meq g^{-1}. With the increasing amount of hydrophilic groups in the membrane, that regions become more inter-connected, leading to more ionic transport channels [43]. Compounds like calcium titanate when treated with bases results in the formation of calcium titanate hydroxide which is an efficient anion exchange material containing exchangeable hydroxyl groups [34]. Calcium titanate can provide a positive surface charge in the membrane which will increase affinity for anions and improve IEC values [44].

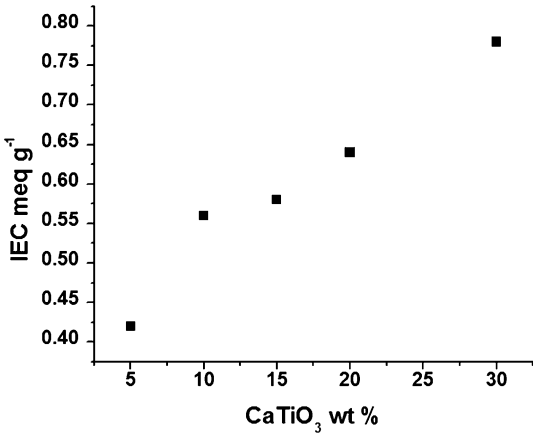

Fig. 8 Ion exchange capacity of membranes with varying $CaTiO_3$ content

Electrical properties

The high ionic conductivity of the anion exchange membrane is an essential property for applications in electrochemical devices. The ionic conductivities were examined by electrochemical impedance spectra (EIS) recorded in the frequency range of 100 Hz–1000 kHz and with signal amplitude of 10 mV. Typical Nyquist plots for the composite membranes are presented in Fig. 9a–e. The membrane resistance was obtained from the intercept on the Z′ axis in the high frequency region. The ionic conductivities of the hydrated PVA/$CaTiO_3$ nanocomposite membranes calculated using the resistance values obtained from the Nyquist plots are shown in Fig. 10. The ionic conductivity is increased from 10.6 mS cm^{-1} for PVA0 to 66 mS cm^{-1} for PVA30 membranes. The ionic conductivity of the membranes largely depends on the nature of inorganic fillers and hydrophilicity of the polymer matrix. High ionic conductivity of PVA/$CaTiO_3$ nanocomposite anion-exchange membranes can be attributed to positive surface charges on $CaTiO_3$ nanoparticles which act as anion exchange sites and enable the exchange of hydroxide ions [44]. The mechanism of anion transport is schematically represented in Fig. 11. The increase in ionic conductivity of the membrane with increasing $CaTiO_3$ content can be attributed to the increase in the positive surface charge of the membrane [34].

Thermo-gravimetric analysis

Thermal stability is an important parameter for the use of membranes in high-temperature electrochemical applications. The samples were heated in the

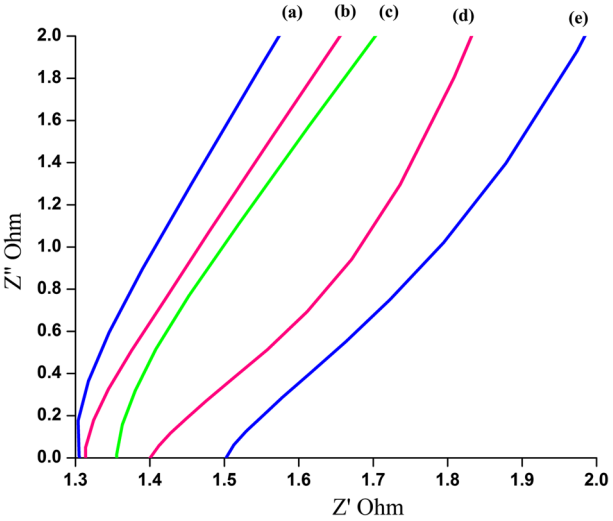

Fig. 9 Nyquist plots from AC impedance spectroscopy measurements of a 2 M NaOH, b PVA30, c PVA20, d PVA10 composite membranes, e PVA membrane

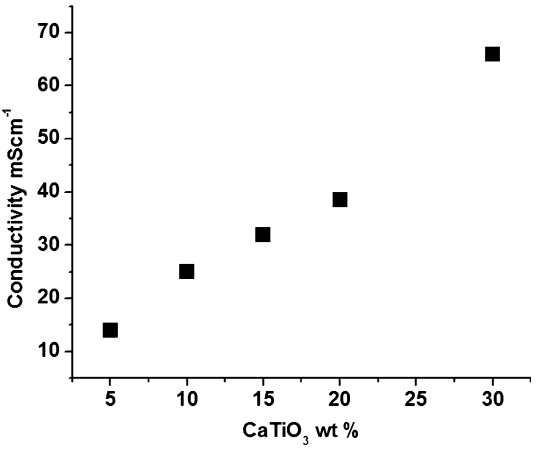

Fig. 10 Ionic conductivity of membranes with varying $CaTiO_3$ content

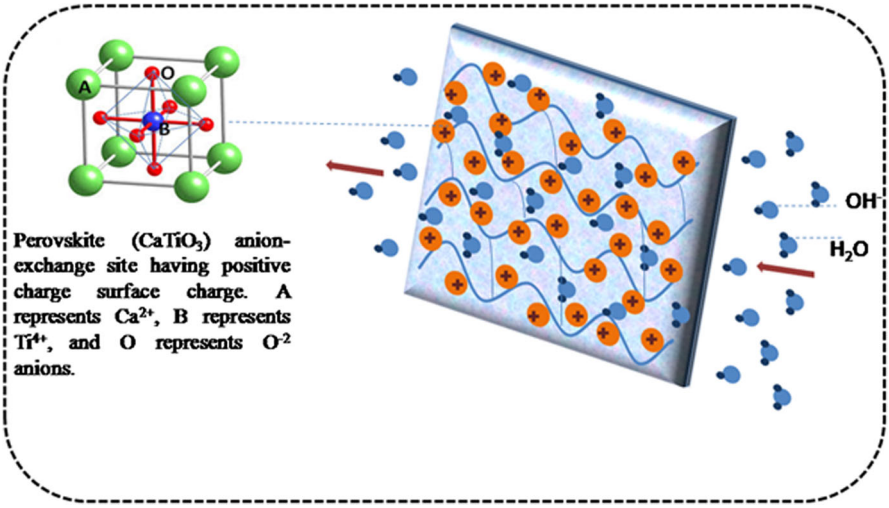

Fig. 11 Schematic representation of PVA/$CaTiO_3$ nanocomposite anion-exchange membrane with $CaTiO_3$ anion-exchange sites that enable high ionic conductivity by providing positive surface charge

temperature range from 30 to 750 °C at a constant rate of 10 °C min^{-1} under nitrogen atmosphere.

Figure 12 shows TGA curves for pure PVA film, PVA10 and PVA30 nanocomposite membranes, respectively. The TGA curve of pure PVA film shows three major weight loss regions. The first region at a temperature of 80–160 °C was associated with the evaporation of weakly adsorbed water and the weight loss of the membrane is about 12.9%. The second region at about 250–350 °C is due to the degradation of PVA polymer membrane and the weight loss of the membrane at this stage is about 61%. The peak of third stage at 450 °C is due to the splitting of PVA chains into small segments, associated with 87.7% weight loss of the membrane. The total weight loss at 600 °C is about 99.1% [18, 25] as listed in Table 2.

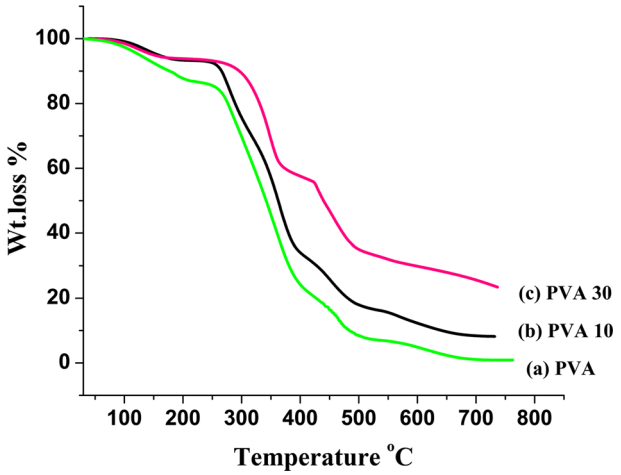

Fig. 12 TGA curves of membranes with varying $CaTiO_3$ content

Table 2 Weight loss % of polymer membranes at different temperatures by TGA analysis

Temperature (°C)	Wt. loss % of membranes		
	PVA	PVA10	PVA30
160	12.9	9.5	9
350	61	48.4	36.7
450	87.7	78	58.6
600	99.1	91.5	73.8

TGA curves of PVA10 and PVA30 nanocomposite polymer membranes also exhibit three major weight loss regions. The first region at a temperature of 80–160 °C is also due to the evaporation of weakly adsorbed water and the weight loss of the membranes is about 9.5%. The second region at 260–350 °C is due to the decomposition of side chain of PVA and glutaraldehyde in the composite membranes, the weight loss of the membrane is only about 48.4% for PVA10 and 36.7% for PVA30. The second main weight loss for the cross-linked PVA/$CaTiO_3$ composite membranes was reduced when compared with that of pure PVA. The peak of third stage at 450 °C is due to the degradation backbone of cross-linked PVA/$CaTiO_3$ polymer membrane. The weight loss of PVA10 was 78 and 58.6% for PVA30. At 600 °C total weight loss for PVA10 is 91.5 and 73.8% for PVA30.

TGA results as shown in Fig. 12 indicate that at each stage the weight loss of PVA membrane is more than that of composite membranes. This suggests that the incorporation of $CaTiO_3$ into PVA matrix and its cross-linking with glutaraldehyde improved thermal stability of the composite membranes [22, 40].

Mechanical properties

AEMs must have good mechanical strength for applications in electrochemical devices. The mechanical strength of composite membranes depends on the filler content [45]. Figure 13 shows the tensile strength (TS) of membranes with varying $CaTiO_3$ content and has the range of 20–46 M Pa. Compared to TS of Nafion-117 (34 M Pa), the prepared composite membranes exhibited better values [42]. As shown in Fig. 13, the TS values increase with filler content up to 20 wt% $CaTiO_3$ and then decrease with increasing filler content.

This shows that appropriate amount of filler content enhances the mechanical properties of PVA composite membrane. It may be attributed to the reduction in degree of crystallinity of the membrane and strengthened filler–matrix interactions [6]. However, an excessive amount of filler content will decrease the mechanical strength of the membranes due to the aggregation of filler particles that act as points of crack propagations [11].

Chemical stability

The chemical stability of anion exchange membranes is an important parameter that affects the performance of electrochemical devices, especially at high pH and strong chemical environments. FT-IR spectrum of the membrane before and after alkaline stability test is presented in Fig. 14a, b. To meet the requirements of the practical applications in strong chemical environments, the prepared AEMs must have good chemical stability, especially in the high pH environments. The results exhibit no significant change in peak positions even after an exposure of membrane in alkaline medium for 2 weeks. The peak in the region 3400–3200 cm^{-1} is intensified due to enhanced hydroxylation of calcium titanate in alkaline environment. In the composite membrane, after alkaline stability test the characteristic vibrations of calcium titanate exhibit no significant change in peak positions. During the alkaline stability test, the membranes did not show any loss of weight. Fenton's reagent is

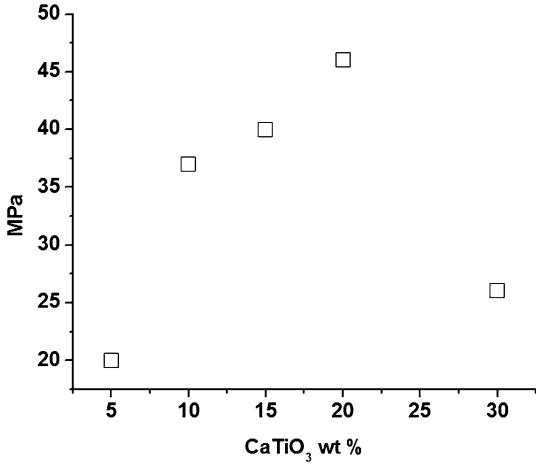

Fig. 13 Tensile strength of membranes with varying $CaTiO_3$ content

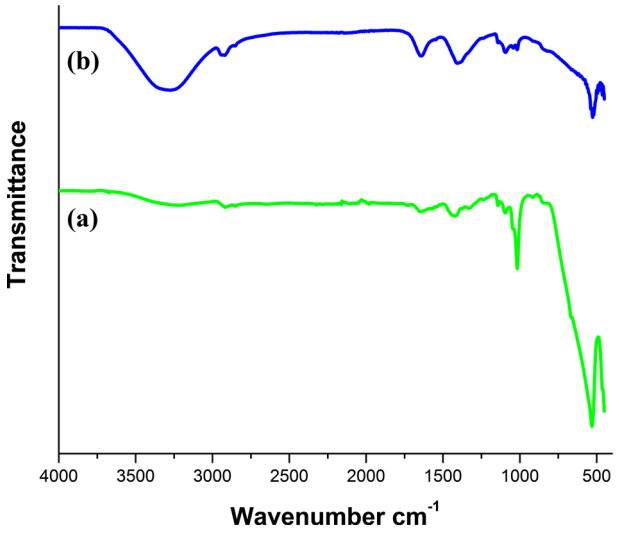

Fig. 14 FT-IR spectrum of the membrane (a) before alkaline stability test, (b) after alkaline stability test

used to simulate and accelerate the harsh operation environment for 24 h, in which the $OH^{\cdot}$ and $OOH^{\cdot}$ radicals formed from H_2O_2 can cause the degradation of the AEMs. All the membranes did not show any physical deformation or colour change and the membrane exhibited a weight loss less than (~ 3%) after 24 h of Fenton's test as shown in Fig. 15. This indicates the adequate oxidative stability of the synthesized membranes under oxidizing conditions.

Performance of $CaTiO_3$/PVA membrane as separator in all-iron flow battery

The cell voltage–time curve measured during the charging and discharging of an all-iron redox flow cell using the prepared membrane as separator is shown in Fig. 16.

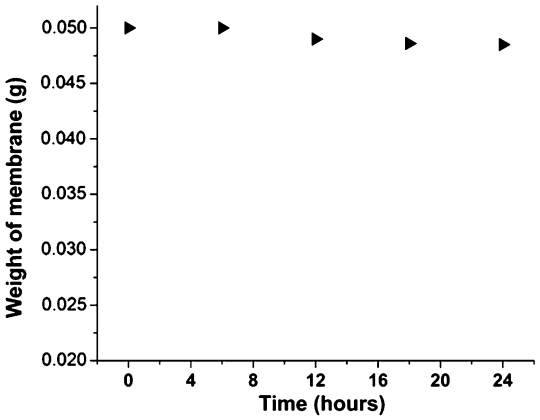

Fig. 15 Weight of membrane with time during Fenton's test

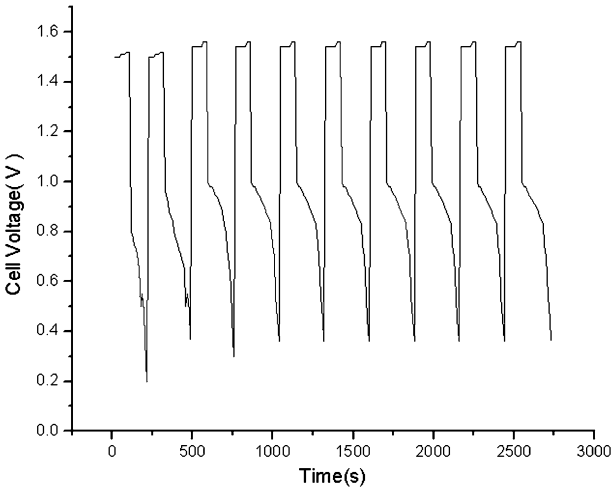

Fig. 16 The cell voltage–time curve of all iron redox flow cell during galvanostatic charge–discharge experiment

A constant current density of 100 mA cm^{-2} for charging and 50 mA cm^{-2} for discharging was used. Repeated charge–discharge measurement of the cell with high-efficiency electrolyte at 100 mA cm^{-2} demonstrated that high coulombic efficiency (> 75%) could be maintained over repeated cycles. Higher coulombic efficiency indicates low cross-mixing of ions [46]. These results confirm the viability of the new composite membrane as a separator in all-iron redox flow battery.

Conclusions

We have reported a novel method to synthesize phase pure calcium titanate nanopowder by co-precipitating mixed oxalate hydroxide of calcium and titanium ($CaTi(OH)_x(C_2O_4)_y$) from a solution of potassium titanyl oxalate and calcium chloride followed by calcination. The XRD pattern revealed the formation of phase pure orthorhombic calcium titanate. The crystalline nature of the particles was also revealed by HRTEM image, and particles are found to be in spherical shape, with an average size of 200 nm. The nanocomposite membrane was fabricated by incorporating calcium titanate into PVA matrix and exhibited improved thermal stability and excellent mechanical properties without compromising ionic conductivity and chemical durability. The results showed that the membrane possessed water uptake and ion exchange properties suitable for AEMs in various electrochemical devices. The composite membrane with 30 wt% of $CaTiO_3$ exhibited maximum conductivity of 66 mS cm^{-1} at room temperature. The galvanostatic charge–discharge tests of all-iron redox flow cell using the PVA/calcium titanate composite membrane as separator exhibited a coulombic efficiency of 75% during repeated charge–discharge cycles.

Acknowledgements P. P. Moly gratefully acknowledges University Grants Commission (UGC) of India for the financial support under Faculty Development Programme, C. B. Jeena and P. J. Elsa are grateful to Council of Scientific and Industrial Research (CSIR), Govt. of India for Research Fellowships.

References

1. Liu Y, Zhang B, Kinsinger CL et al (2016) Anion exchange membranes composed of a poly(2,6-dimethyl-1,4-phenylene oxide) random copolymer functionalized with a bulky phosphonium cation. J Membr Sci 506:50–59. https://doi.org/10.1016/j.memsci.2016.01.042
2. Pupkevich V, Glibin V, Karamanev D (2013) Phosphorylated polyvinyl alcohol membranes for redox Fe^{3+}/H_2 flow cells. J Power Sources 228:300–307. https://doi.org/10.1016/j.jpowsour.2012.11.080
3. Kariduraganavar MY, Nagarale RK, Kittur AA, Kulkarni SS (2006) Ion-exchange membranes: preparative methods for electrodialysis and fuel cell applications. Desalination 197:225–246. https://doi.org/10.1016/j.desal.2006.01.019
4. Lee KP, Arnot TC, Mattia D (2011) A review of reverse osmosis membrane materials for desalination—development to date and future potential. J Membr Sci 370:1–22. https://doi.org/10.1016/j.memsci.2010.12.036
5. Zeng L, Zhao TS, Li YS (2012) Synthesis and characterization of crosslinked poly (vinyl alcohol)/layered double hydroxide composite polymer membranes for alkaline direct ethanol fuel cells. Int J Hydrogen Energy 7:1–8. https://doi.org/10.1016/j.ijhydene.2012.09.089
6. Nishimura M, Higa M, Akamine K, Masudaya S (2008) Preparation and characterization of anion-exchange membranes with a semi-interpenetrating network structure of poly (vinyl alcohol) and poly (allyl amine). Desalination 233:157–165. https://doi.org/10.1016/j.desal.2007.09.038
7. Qiu J, Li M, Ni J et al (2007) Preparation of ETFE-based anion exchange membrane to reduce permeability of vanadium ions in vanadium redox battery. J Membr Sci 297:174–180. https://doi.org/10.1016/j.memsci.2007.03.042
8. Di Vona ML, Narducci R, Pasquini L et al (2014) Anion-conducting ionomers: study of type of functionalizing amine and macromolecular. Int J Hydrogen Energy 39:14039–14049. https://doi.org/10.1016/j.ijhydene.2014.06.166
9. Koo JS, Kwak N, Sung T (2012) Synthesis and properties of an anion-exchange membrane based on vinylbenzyl chloride–styrene–ethyl methacrylate copolymers. J Membr Sci 423–424:293–301. https://doi.org/10.1016/j.memsci.2012.08.024
10. Zeng R, Varcoe J (2011) Alkaline anion exchange membranes for fuel cells—a patent review. Recent Patents Chem Eng 44:1–50
11. Merle G, Wessling M, Nijmeijer K (2011) Anion exchange membranes for alkaline fuel cells: a review. J Membr Sci 377:1–35. https://doi.org/10.1016/j.memsci.2011.04.043
12. Lin X, Wu L, Liu Y et al (2012) Alkali resistant and conductive guanidinium-based anion-exchange membranes for alkaline polymer electrolyte fuel cells. J Power Sources 217:373–380. https://doi.org/10.1016/j.jpowsour.2012.05.062
13. Sajjad SD, Liu D, Wei Z et al (2015) Guanidinium based blend anion exchange membranes for direct methanol alkaline fuel cells (DMAFCs). J Power Sources 300:95–103. https://doi.org/10.1016/j.jpowsour.2015.08.002
14. Smitha B, Sridhar S, Khan AA (2005) Solid polymer electrolyte membranes for fuel cell applications—a review. J Membr Sci 259:10–26. https://doi.org/10.1016/j.memsci.2005.01.035
15. Sharma S, Dinda M, Sharma CR, Ghosh PK (2014) A safer route for preparation of anion exchange membrane from inter-polymer film and performance evaluation in electrodialytic application. J Membr Sci 459:122–131. https://doi.org/10.1016/j.memsci.2014.02.011
16. Mizutani Y (1990) Structure of ion exchange membranes. J Membr Sci 49:121–144. https://doi.org/10.1016/S0376-7388(00)80784-X
17. Thomas OD, Soo KJWY, Peckham TJ et al (2012) A stable hydroxide-conducting polymer. J Am Chem Soc 10753–10756. https://doi.org/10.1021/ja303067t
18. Yang C (2006) Synthesis and characterization of the cross-linked PVA/TiO_2 composite polymer membrane for alkaline DMFC. J Membr Sci 51–60. https://doi.org/10.1016/j.memsci.2006.10.048
19. Faraj M, Elia E, Boccia M et al (2011) New anion conducting membranes based on functionalized styrene–butadiene–styrene triblock copolymer for fuel cells applications. J Polym Sci Part A Polym Chem 49:3437–3447. https://doi.org/10.1002/pola.24781

20. Wang X (2011) Preparation of alkaline anion exchange polymer membrane from methylated melamine grafted poly (vinylbenzyl chloride) and its fuel cell performance. J Mater Chem 12910–12916. https://doi.org/10.1039/c1jm12068a
21. Wu H, Jia W, Liu Y (2017) An imidazolium-type hybrid alkaline anion exchange membrane with improved membrane stability for alkaline fuel cells applications. J Mater Sci 52:1704–1716. https://doi.org/10.1007/s10853-016-0462-y
22. Yang CC, Chiu SJ, Chien WC, Chiu SS (2009) Quaternized poly(vinyl alcohol)/alumina composite polymer membranes for alkaline direct methanol fuel cells. J Power Sources 195:2212–2219. https://doi.org/10.1016/j.jpowsour.2009.10.091
23. Chang HY, Lin CW (2003) Proton conducting membranes based on PEG/SiO_2 nanocomposites for direct methanol fuel cells. J Membr Sci 218:295–306. https://doi.org/10.1016/S0376-7388(03)00187-X
24. Sang S, Zhang J, Wu Q, Liao Y (2007) Influences of Bentonite on conductivity of composite solid alkaline polymer electrolyte PVA–Bentonite–KOH–H_2O. Electrochim Acta 52:7315–7321. https://doi.org/10.1016/j.electacta.2007.06.004
25. Heydari M, Moheb A, Ghiaci M, Masoomi M (2013) Effect of cross-linking time on the thermal and mechanical properties and pervaporation performance of poly(vinyl alcohol) membrane cross-linked with fumaric acid used for dehydration of isopropanol. J Appl Polym Sci 128:1640–1651. https://doi.org/10.1002/app.38264
26. De Oliveira AHP, Nascimento MLF, De Oliveira HP (2016) Preparation of KOH-doped PVA/PSSA solid polymer electrolyte for DMFC: the influence of TiO 2 and PVP on performance of membranes. Fuel Cells 1–6. https://doi.org/10.1002/fuce.201500199
27. Ran J, Wu L, He Y et al (2017) Ion exchange membranes: new developments and applications. J Membr Sci 522:267–291. https://doi.org/10.1016/j.memsci.2016.09.033
28. Zheng H, Reaney IM, Csete de Gyorgyfalva CDC (2004) Raman spectroscopy of $CaTiO_3$-based perovskite. J Mater Res 19:488–495
29. Zheng H, Bagshaw H, Csete de Gyrgyfalva GDC et al (2003) Raman spectroscopy and microwave properties of $CaTiO_3$-based ceramics. J Appl Phys 94:2948–2956. https://doi.org/10.1063/1.1598271
30. Demirors AF, Imhof A (2009) $BaTiO_3$, $SrTiO_3$, $CaTiO_3$, and $Ba_xSr_{1-x}TiO_3$ particles: a general approach for monodisperse colloidal perovskites. Chem Mater 21:3002–3007. https://doi.org/10.1021/cm900693r
31. Marques VS, Cavalcante LS, Sczancoski JC et al (2009) Synthesis of (Ca, Nd)TiO3 powders by complex polymerization, Rietveld refinement and optical properties. Spectrochim Acta Part A Mol Biomol Spectrosc 74:1050–1059. https://doi.org/10.1016/j.saa.2009.08.049
32. Dubey AK, Basu B, Balani K et al (2011) Multifunctionality of perovskites $BaTiO_3$ and $CaTiO_3$ in a composite with hydroxyapatite as orthopedic implant materials. Integr Ferroelectr 131:119–126. https://doi.org/10.1080/10584587.2011.616425
33. Sharma YK, Kharkwal M, Uma S, Nagarajan R (2009) Synthesis and characterization of titanates of the formula MTiO3 (M = Mn, Fe, Co, Ni and Cd) by co-precipitation of mixed metal oxalates. Polyhedron 28:579–585. https://doi.org/10.1016/j.poly.2008.11.056
34. Urbain OM, Stemeri WR, Charles H (1940) United States "Patent. Office 7". US Pat. 2208173
35. Manohar AK, Kim KM, Plichta E et al (2016) JES focus issue on redox flow batteries—reversible fuel cells a high efficiency iron-chloride redox flow battery for large-scale energy storage. J Electrochem Soc 163:5118–5125. https://doi.org/10.1149/2.0161601jes
36. Rai AK, Rao KN, Kumar LV, Mandal KD (2009) Synthesis and characterization of ultra fine barium calcium titanate, barium strontium titanate and $Ba_{1-2x}Ca_x$ Sr_xTiO_3 (x = 0.05, 0.10). J Alloys Compd 475:316–320. https://doi.org/10.1016/j.jallcom.2008.07.038
37. Dong W, Zhao G, Bao Q, Gu X (2015) Solvothermal preparation of $CaTiO_3$ prism and $CaTi_2O_4(OH)_2$ nanosheet by a facile surfactant-free method. Mater Sci (MEDŽIAGOTYRA) 21:583–585. https://doi.org/10.5755/j01.ms.21.4.9697
38. Wang ED, Zhao TS, Yang WW (2010) Poly (vinyl alcohol)/3-(trimethylammonium) propyl-functionalized silica hybrid membranes for alkaline direct ethanol fuel cells. Int J Hydrogen Energy 35:2183–2189. https://doi.org/10.1016/j.ijhydene.2009.12.179
39. AL-Sabagh AM, Abdeen Z (2010) Preparation and characterization of hydrogel based on poly(vinyl alcohol) cross-linked by different cross-linkers used to dry organic solvents. J Polym Environ 18:576–583. https://doi.org/10.1007/s10924-010-0200-5

40. Xiong Y, Liu QL, Zhu AM et al (2009) Performance of organic–inorganic hybrid anion-exchange membranes for alkaline direct methanol fuel cells. J Power Sources 186:328–333. https://doi.org/10.1016/j.jpowsour.2008.10.070
41. Fu R, Woo J, Seo S et al (2008) Covalent organic/inorganic hybrid proton-conductive membrane with semi-interpenetrating polymer network: preparation and characterizations. J Power Sources 179:458–466. https://doi.org/10.1016/j.jpowsour.2007.12.118
42. Pandey J, Mir FQ, Shukla A (2014) Synthesis of silica immobilized phosphotungstic acid (Si-PWA)-poly (vinyl alcohol) (PVA) composite ion-exchange membrane for direct methanol fuel cell. Int J Hydrogen Energy 1–9. https://doi.org/10.1016/j.ijhydene.2014.03.237
43. Ran J, Wu L, Varcoe JR et al (2012) Development of imidazolium-type alkaline anion exchange membranes for fuel cell application. J Membr Sci 415–416:242–249. https://doi.org/10.1016/j.memsci.2012.05.006
44. Wiff JP, Fuenzalida VM, Arias JL, Fernandez MS (2007) Hydrothermal-electrochemical $CaTiO_3$ coatings as precursor of a biomimetic calcium phosphate layer. Mater Lett 61:2739–2743. https://doi.org/10.1016/j.matlet.2006.06.092
45. Musse C, Sharma S, Madalena M et al (2016) New approaches towards novel composite and multilayer membranes for intermediate temperature-polymer electrolyte fuel cells and direct methanol fuel cells. J Power Sources 316:139–159. https://doi.org/10.1016/j.jpowsour.2016.03.052
46. Li X, Zhang H, Mai Z et al (2011) Ion exchange membranes for vanadium redox flow battery (VRB) applications. Energy Environ Sci 4:1147. https://doi.org/10.1039/c0ee00770f